Neurobiology of Disease

Nascent Aβ42 Fibrillization in Synaptic Endosomes Precedes Plaque Formation in a Mouse Model of Alzheimer's-like β-Amyloidosis

Elizabeth A. Eckman,[1] Dana M. Clausen,[1] Santiago Solé-Domènech,[2] Chris W. Lee,[1] Cristina Sinobas-Pereira,[3] Ryan J. Domalewski,[3] Michael R. Nichols,[3] and Javier Pacheco-Quinto[1]

[1]Biomedical Research Institute of New Jersey, Cedar Knolls, New Jersey 07927, [2]Department of Biochemistry, Weill Cornell Medical College, New York, New York 10065, and [3]Department of Chemistry & Biochemistry, University of Missouri–St. Louis, St. Louis, Missouri 63121

Accumulation of amyloid-β peptide (Aβ) aggregates in synapses may contribute to the profound synaptic loss characteristic of Alzheimer's disease (AD). The origin of synaptic Aβ aggregates remains elusive, but loss of endosomal proteostasis may trigger their formation. In this study, we identified the synaptic compartments where Aβ accumulates, and performed a longitudinal analysis of synaptosomes isolated from brains of TgCRND8 APP transgenic mice of either sex. To evaluate the specific contribution of Aβ-degrading protease endothelin-converting enzyme (ECE-1) to synaptic/endosomal Aβ homeostasis, we analyzed the effect of partial *Ece1* KO in brain and complete *ECE1* KO in SH-SY5Y cells. Global inhibition of ECE family members was used to further assess their role in preventing synaptic Aβ accumulation. Results showed that, before extracellular amyloid deposition, synapses were burdened with detergent-soluble Aβ monomers, oligomers, and fibrils. Levels of all soluble Aβ species declined thereafter, as Aβ42 turned progressively insoluble and accumulated in Aβ-producing synaptic endosomal vesicles with characteristics of multivesicular bodies. Accordingly, fibrillar Aβ was detected in brain exosomes. ECE-1-deficient mice had significantly increased endogenous synaptosomal Aβ42 levels, and protease inhibitor experiments showed that, in TgCRND8 mice, synaptic Aβ42 became nearly resistant to degradation by ECE-related proteases. Our study supports that Aβ accumulating in synapses is produced locally, within endosomes, and does not require the presence of amyloid plaques. ECE-1 is a determinant factor controlling the accumulation and fibrillization of nascent Aβ in endosomes and, in TgCRND8 mice, Aβ overproduction causes rapid loss of Aβ42 solubility that curtails ECE-mediated degradation.

Key words: Alzheimer's disease; amyloid; endosomes; endothelin-converting enzyme-1; exosomes; synapse

Significance Statement

Deposition of aggregated Aβ in extracellular plaques is a defining feature of AD. Aβ aggregates also accumulate in synapses and may contribute to the profound synaptic loss and cognitive dysfunction typical of the disease. However, it is not clear whether synaptotoxic Aβ is mainly derived from plaques or if it is produced and aggregated locally, within affected synaptic compartments. Filling this knowledge gap is important for the development of an effective treatment for AD, as extracellular and intrasynaptic pools of Aβ may not be equally modulated by immunotherapies or other therapeutic approaches. In this manuscript, we provide evidence that Aβ aggregates building up in synapses are formed locally, within synaptic endosomes, because of disruptions in nascent Aβ proteostasis.

Received June 26, 2023; revised Oct. 5, 2023; accepted Oct. 23, 2023.

Author contributions: E.A.E., S.S.-D., C.W.L., M.R.N., and J.P.-Q. designed research; E.A.E., D.M.C., S.S.-D., C.W.L., C.S.-P., R.J.D., M.R.N., and J.P.-Q. analyzed data; E.A.E., D.M.C., S.S.-D., M.R.N., and J.P.-Q. edited the paper; E.A.E. and J.P.-Q. wrote the paper; E.A.E., D.M.C., S.S.-D., C.W.L., C.S.-P., R.J.D., and J.P.-Q. performed research.

This work was supported in part by the Vanech Family Foundation to E.A.E. and J.P.-Q.; University of Missouri FastTrack Award to M.R.N.; and National Institutes of Health R15GM119070 to M.R.N. S.S.-D. was supported by Cure Alzheimer's Foundation Grant CAF-211540-02, Swedish Research Council International Postdoctoral Fellowship 637-2013-503/D0050301, and Leon Levy Foundation Fellowship in Neuroscience. We thank Hui Peng (Biomedical Research Institute of New Jersey) for technical support; and Luis Marcelino (Biomedical Research Institute of New Jersey) for help with animal husbandry.

The authors declare no competing financial interests.

Correspondence should be addressed to Javier Pacheco-Quinto at pacheco-quinto@brinj.org or Elizabeth A. Eckman at lizeckman@brinj.org.

https://doi.org/10.1523/JNEUROSCI.1318-23.2023

Introduction

Disruption of endosomal/lysosomal (E/L) function is recognized as a possible precipitating factor for the development of brain β-amyloidosis, a condition caused by the abnormal aggregation of β-amyloid peptide (Aβ) and one of the main neuropathological features of Alzheimer's disease (AD) (Glenner and Wong, 1984; Roychaudhuri et al., 2009). The role that endosomes play in homeostasis of Aβ is twofold. First, Aβ is produced by cleavage of the amyloid precursor protein (APP) within neuronal endosomal vesicles and perturbations in vesicular pH and trafficking can greatly enhance Aβ production (Nixon, 2007; Pacheco-Quinto and Eckman, 2013; Pacheco-Quinto et al., 2019). Second,

the E/L pathway is a major catabolic route for Aβ and contains multiple proteases, including cathepsins and endothelin-converting enzymes (ECE) -1 and -2, that prevent buildup of the peptide. Alterations in the endosomal system therefore have the potential to impact both Aβ production and degradation, leading to excess accumulation of intracellular Aβ and its aggregation (Pacheco-Quinto and Eckman, 2013), a required step for the development of amyloid pathology. Indeed, increased intraneuronal Aβ immunoreactivity (Gyure et al., 2001; Mori et al., 2002; Cataldo et al., 2004; Billings et al., 2005; Pensalfini et al., 2014) and signs of E/L dysfunction, such as enlarged and poorly acidified endosomal vesicles, are evident before the onset of extracellular pathology (Cataldo et al., 1994; Nixon, 2017; Lee et al., 2022).

Synaptic dysfunction is another early feature of AD and is considered, in part, to be an Aβ-driven insult. Numerous studies have demonstrated that soluble Aβ aggregates can interfere with normal synaptic function and cause synaptic degeneration (S. Li and Selkoe, 2020). How neurotoxic Aβ aggregates develop and reach synapses in the first place is still unclear, but evidence suggesting a potential endogenous intraneuronal origin is compelling. Neuronal endosomes are the main Aβ-producing compartments in brain, provide a favorable environment for Aβ aggregation, and in synapses, accumulation of Aβ in endosomes is a characteristic ultrastructural finding in AD (Takahashi et al., 2002; Langui et al., 2004). Hence, similar to the inside-out hypothesis for plaque formation (Gouras et al., 2014), progressive synaptic degeneration could be driven by excess accumulation of Aβ produced within synaptic endosomes.

In this study, using a mouse model of AD-like β-amyloidosis, we conducted a longitudinal biochemical analysis of synaptic Aβ accumulation and explored early changes in intraneuronal Aβ proteostasis contributing to the pathologic process. The results of these experiments, paired with additional data from ECE-1-deficient cells and mice, provide new insights on the origin of intrasynaptic Aβ aggregates and demonstrate that loss of endosomal Aβ homeostasis may be a major driver of amyloid pathology in AD.

Materials and Methods

Mice. TgCRND8 mice were a kind gift from Paul Fraser, University of Toronto (Chishti et al., 2001). All experimental mice were obtained by breeding male TgCRND8 mice and female B6C3F1/J hybrid mice (stock #100010, The Jackson Laboratory). *Ece1*$^{tm1a(KOMP)Wtsi}$ mice, generated by the Knock-out Mouse Project (KOMP) and obtained from the Mutant Mouse Resource & Research Centers at the University of California–Davis (MMRRC:047475-UCD), contain a "knock-out first" reporter-tagged insertion allele. Humanized *App* knock-in mice (B6 (SJL)-*App*$^{tm1.1Aduci}$/J) (Baglietto-Vargas et al., 2021) were obtained from The Jackson Laboratory (RRID:IMSR_JAX:030898) and were used to prepare synaptosomes for establishing background signal in rodent-specific Aβ ELISAs. All mice were housed in ventilated micro-isolator cages with unrestricted access to food and water and were provided with nesting material and Shepherd shacks (Shepherd Specialty Papers). The housing room was under a 12 h/12 h light/dark cycle with controlled temperature and humidity. The use of mice was approved by the Institutional Animal Care and Use Committee at BRInj and followed American Veterinary Medical Association guidelines.

Synaptosomal preparations. Mice were killed by CO_2 asphyxiation, brains removed, and cortex and hippocampus quickly dissected. Tissue was placed on ice in cold 0.32 M sucrose/10 mM HEPES buffer containing protease inhibitor cocktail with EDTA (50 mg wet weight per ml) and was homogenized with 10 strokes of a motorized glass-Teflon Dounce homogenizer. From the crude homogenate, an aliquot was kept for measuring total Aβ. The interstitial enriched "extracellular" extract was prepared as the final supernatant from three sequential centrifugation steps at 4°C (1000 × *g* for 10 min, 16,000 × *g* for 10 min, 100,000 × *g* for 1 h). Crude synaptosomes were pelleted at the 16,000 × *g* centrifugation step and were washed 3 times by cycles of resuspension in homogenization buffer and centrifugation at 16,000 × *g* for 10 min at 4°C. Washed synaptosomal pellets from 1 ml homogenate were then lysed in 1 ml RIPA buffer (25 mM Tris-HCl, 150 mM NaCl, 1% NP-40, 1% sodium deoxycholate, 0.1% SDS, pH 7.6) containing Halt Protease Inhibitor Cocktail with EDTA (Fisher Scientific) and centrifuged at 16,000 × *g* for 10 min to obtain the soluble fraction. Insoluble Aβ was extracted from the resulting pellet by addition of 50 µl of 6 M guanidine-HCl (GuHCl). For extraction of total Aβ, crude homogenates were diluted 1:20 in 6 M GuHCl and incubated for 30 min at room temperature. For analysis of endogenous rodent Aβ in *Ece1* (+/+) and (+/−) mice, crude synaptosomes were prepared essentially as described above from brains homogenized at 100 mg wet weight per ml. Washed synaptosomal pellets were extracted directly with 1/10 volume 6 M GuHCl (relative to original homogenate volume) for 1 h at room temperature, and extracts were diluted 1:15 in ELISA binding buffer before analysis. For ECE-1 activity assays, synaptosomes were prepared in the absence of EDTA.

To obtain a pure synaptosomal fraction, crude synaptosomal pellets were loaded on to a 0.6-16 M continuous sucrose gradient and spun for 18 h in a swinging bucket rotor at 165,000 × *g* at rMAX. From the top to bottom, 500 µl fractions were collected, diluted 5 times with 10 mM HEPES, and spun down at 16,000 × *g*. For the separation of vesicles contained in synaptosomes, pelleted synaptosomes were subjected to osmotic shock by incubation in 10 mM HEPES for 20 min at 4°C. The solution was then passed through a 25-gauge needle and loaded onto a 5%-25% Optiprep (D1556, Millipore Sigma) continuous gradient and spun for 2 h at 140,000 × *g* at rMAX in a swinging bucket rotor. Aliquots of 500 µl were collected starting from the top.

Thioflavin staining protocol. Brains fixed in 10% neutral buffered formalin were embedded in paraffin and processed into 10-µm-thick sagittal sections. For each mouse, 3 slides, 100 µm apart, were used to assess amyloid plaques. Slides were deparaffinized and rehydrated by incubation at 60°C for 60 min followed by 5 min incubations in xylene (3 times), 100% ethanol, 95% ethanol, 50% ethanol and water. Slides were incubated in 5% thioflavin T in water (T3516, Millipore Sigma), rinsed with water, incubated in 1% acetic acid solution for 15 min, rinsed, air dried, and mounted. Plaques were visualized with a Zeiss Axio Imager Z1 fluorescent microscope, and all plaques present in cortex and hippocampus were counted manually.

Isolation of brain exosomes. Exosome-enriched extracellular vesicles (EVs) were isolated from dissected cortex/hippocampus using previously described methods with few modifications (Perez-Gonzalez et al., 2017). Half brains were mildly dissociated with 20 U/ml papain (#LK00316; Worthington Biochemical) and centrifuged sequentially at 1000 × *g* (to pellet cell debris), 10,000 × *g* (to sediment other EVs, such as macrovesicles or ectosomes), followed by a 100,000 × *g* ultracentrifugation step to pellet extracellular exosomes. Pellets then were resuspended in PBS and loaded on top of a discontinuous sucrose gradient (0.25, 0.6, 0.95, 1.3, 1.65 M sucrose) and centrifuged for 16 h at 200,000 × *g*. Based on their density, exosomes equilibrate at the 0.6/0.95 M sucrose interlayer (1.08-1.13 × *g*/ml density) and produce a visible layer. Using a syringe needle, the exosome layer was extracted, diluted with PBS buffer, and centrifuged again at 100,000 × *g* to pellet exosomes. Exosomes were resolubilized in 30 µl saline buffer to obtain an average protein concentration of 4 mg/ml. The size of the EVs was measured by Dynamic Light Scattering using a Malvern Zetasizer Nano ZS (Malvern Instruments). Preparations were diluted in 25 mM trehalose to obtain three independent measures.

Intracerebroventricular injection. Mice under isoflurane anesthesia (1.5%-5%) were placed in a stereotaxic frame (Stoelting), with body temperature maintained with a heating pad. A dental drill was used to perforate the skull (0.9 mm posterior, 1.5 mm lateral to bregma) and 2 µl of phosphoramidon (118 nmol) or vehicle (0.9% saline), were administered into each lateral ventricle (depth 2.1 mm) at rate of 0.5 µl/minute with a Hamilton glass microsyringe driven by a microsyringe pump (World Precision Instruments). Before surgery, bupivacaine (0.1 ml of a 0.125% solution) was injected subcutaneously at the incision site and meloxicam

(2 mg/kg, i.p.) was administered for analgesia. Related data from a subset of the injected mice were reported in a previous publication (Pacheco-Quinto et al., 2019).

Cell culture. Human neuroblastoma SH-SY5Y cells (ATCC CRL-2266, RRID:CVCL_0019, American Type Culture Collection) stably transfected with pcDNA3 (Invitrogen) containing nonmutant human APP_{695} cDNA (NM_201414.2) were maintained in DMEM supplemented with 10% FBS and penicillin and streptomycin, and routinely passed by trypsinization. To quantify Aβ by ELISA, cells were grown in 12-well plates and treated with 100 μM of phosphoramidon and/or E-64 (Millipore Sigma) for 48 h and extracted with 100 μl of RIPA buffer (25 mM Tris-HCl, 150 mM NaCl, 1% NP-40, 1% sodium deoxycholate, 0.1% SDS, pH 7.6) containing Halt Protease Inhibitor Cocktail with EDTA (Fisher Scientific). After a 10 min incubation on ice, samples were spun at 16,000 × *g* and supernatant was used to measure RIPA-soluble Aβ42. The remaining pellet was incubated with 20 μl of 6 M GuHCl at room temperature for 30 min and then diluted by addition of 80 μl RIPA. Extracts were further diluted 1:4 in binding buffer before analysis by ELISA.

Generation of ECE1 KO in SH-SY5Y-APP cells. Guide RNA targeting sequence oligos 1 (sgRNA-ECE1ex4-1, 5′-CACCGCTGAGACACAAG CTTCGCTC-3′) and 2 (sgRNA-ECE1ex4-2, 5′-CACCGCCCTGATG GCCACTCACGCT) were individually subcloned into pSpCas9(BB)-2A-Puro (PX459) version 2.0, a gift from Feng Zhang (Ran et al., 2013) (Addgene plasmid #62988; http://n2t.net/addgene:62988; RRID:Addgene_62988). *ECE1* targeting sequences were tested by the Off-Spotter software to minimize potential off target effects. SH-SH5Y-APP cells were cotransfected with the vectors using Lipofectamine 3000 transfection reagent (Fisher Scientific), and placed under puromycin (2.5 μg/ml) selection for 4 d. After 4 weeks, individual colonies were isolated and expanded; clones with genomic insertions/deletions resulting in frameshifts were identified by Sanger DNA sequencing (Genewiz). APP expression level was determined by Western blot compared with the parent SH-SY5Y-APP line. Phenotypes of three clones with unique insertions/deletions were assessed by measuring Aβ levels in culture medium and cell lysate after 24 h incubation ± 100 μM phosphoramidon. All clones were insensitive to phosphoramidon treatment, but some had reduced APP expression, compared with the parent line, after clonal selection (data not shown). For all subsequent experiments in this study, we used a clone with APP expression similar to that of the parent line, that had cleavage on the target sites creating a 131 bp deletion in *ECE1*, resulting in a premature stop codon. Absence of ECE-1 activity in this clone was confirmed using a big ET-1 conversion assay.

ECE-1 enzymatic activity. Cell membrane fractions were prepared as described by Xu et al. (1994). Cell membranes, or mouse brain synaptosomes, were solubilized in 20 mM Tris-HCl containing 250 mM sucrose and 2.5% $C_{12}E_{10}$ (polyoxyethylene-10-lauryl ether, Millipore Sigma). Protein concentration was measured using Pierce BCA assay kit (Fisher Scientific). ECE-1 activity was quantified using a big ET-1 conversion assay (Emoto and Yanagisawa, 1995). Briefly, 2.5 μg protein were incubated for 20 min at 37°C with 0.1 μM human big endothelin-1 (big ET-1 1-38) peptide (Enzo Life Sciences) in 50 mM acetic acid, 50 mM 2-(N-morpholino)ethanesulfonic acid, 100 mM Tris, pH 6.8 (Fahnoe et al., 2000), containing Halt Protease Inhibitor Cocktail (Fisher Scientific) and 1 μM thiorphan (Cayman Chemical). Parallel reactions were conducted in the presence of 100 μM phosphoramidon. After stopping the reactions by addition of 5 mM EDTA, mature ET-1 (1-21) peptide was measured by sandwich ELISA (Endothelin-1 Quantikine ELISA kit, R&D Systems).

Immunocytochemistry and microscopy. SH-SY5Y-APP cells grown on glass coverslips were fixed with cold methanol at −20°C for 10 min. Cells were then incubated with 5% BSA/PBS containing 0.05% Triton X-100 for 30 min at room temperature, followed by a 4°C overnight incubation with anti-Aβ1-16 antibody MM27-33.1.1 (also known as Ab3, QED Bioscience, catalog #57003) (1:500) for Aβ detection or anti-amyloid fibrils OC antiserum (EMD Millipore, catalog #AB2286, RRID:AB_1977024) (1:500) for detection of fibrillar species. Anti-mouse or anti-rabbit antibodies conjugated with AlexaFluor-488 (Invitrogen) were used for detection. Nuclei were stained with Hoechst 33258 (Anaspec). For OC colocalization studies, cells were fixed with 10% PFA and permeabilized with 0.1% Triton X-100. OC signal was detected with an anti-rabbit AlexaFluor-546 antibody in cells incubated overnight with 0.5 μg/ml Lucifer yellow (Millipore Sigma) to visualize the endocytic pathway, or in cells transiently transfected with CD63-pEGFP C2 (gift from Paul Luzio, Addgene plasmid #62964; http://n2t.net/addgene:62964; RRID:Addgene_62964) using Lipofectamine 3000. For colocalization with a late endosomal marker, dual immunofluorescence was performed with OC antiserum and mouse anti-Rab7 (E9O7E, Cell Signaling catalog #95746, RRID:AB_2800252). Fluorescent signal was visualized with a Zeiss Axio Imager Z1 fluorescent microscope.

For super resolution imaging, we used a Zeiss LSM880 confocal microscope equipped with Airyscan. Fields of interest were visualized with a 63× oil objective (NA 1.4) and the Airyscan Super Resolution mode. Hoechst and AlexaFluor-488 were excited using the 405 and 488 nm laser lines, respectively. Sixteen-bit stacks were acquired at 1000 × 1000 pixel frames with pixel dwell times of 2.06 μs. Acquired stacks were processed through using linear deconvolution of each of the 32 individual elements to enhance their lateral and axial resolution, followed by pixel reassignment of each element back to the center position. Airyscan filtering (Wiener filter associated with deconvolution) was set to the default value of 6.0 for 2D images. Maximal projections of stacks were prepared using Fiji digital imaging software.

ELISA. Aβ was measured by sandwich ELISA as previously described (Scheuner et al., 1996) using antibody pairs that detect monomeric peptides preferentially, or that detect oligomers. For quantification of human or mouse Aβ1-40, Aβ was captured with N-terminal antibody MM27-33.1.1 (also known as Ab3, QED Bioscience, catalog #57003) or M3.2 (Biolegend catalog #805701, RRID:AB_2564982), respectively, and detected with HRP-conjugated Aβ40-specific antibody MM32-13.1.1 (also known as Ab40.1, QED Bioscience, catalog #57002). For quantification of Aβ ending at position 42, both human and mouse Aβ were captured with Aβ42-specific antibody MM26-2.1.3 (also known as Ab42.2, QED Bioscience, catalog #57001) and detected with HRP-conjugated 4G8 (Biolegend, catalog #800720, RRID:AB_2783372). This Aβ42 assay recognizes N-terminally truncated peptides in addition to full-length Aβ1-42. An alternative Aβ42 sandwich ELISA (capture with anti-rodent Aβ 1-16 antibody M3.2 and detection with anti-Aβ42 antibody BC05 (Fujifilm Wako #014-26903) was used to measure endogenous Aβ42 in synaptosomes from *Ece1* (+/−) mice.

Aβ oligomers were quantified using a commercial sandwich ELISA that uses N-terminal antibody MOAB-2 for both capture and detection (Biosensis, catalog #BEK-2215) and preferentially detects oligomers (Tai et al., 2013).

Aβ protofibrils were quantified with a sandwich ELISA composed of protofibril-selective monoclonal capture antibody (mAbSL113) and a biotinylated affinity-purified protofibril-selective detection antibody (apAbSL40-4). The assay was completed by addition of a streptavidin-HRP conjugate, and HRP colorimetric substrates. A standard curve of isolated Aβ42 protofibrils ranging from 0.16 to 10 nM (705-45,140 pg/ml) was constructed, and protofibril concentrations in the samples were determined from linear regression of the protofibrils standard absorbances. R^2 values for the standard curves were typically >0.99. The antibodies, modifications, and sandwich ELISA were developed at the University of Missouri–St. Louis, the basis of which was reported previously (Colvin et al., 2017; Grover et al., 2023).

For analysis of extracellular-enriched TgCRND8 mouse brain extracts, 100 μl extract were added to wells containing 50 μl ELISA binding buffer (0.02 M sodium phosphate, pH 7.0, containing 0.002 M EDTA, 0.4 M NaCl, 0.2% BSA, 0.05% 3-[(3-cholamidopropyl)dimethylammonio]-1-propanesulfonate, 0.4% Block Ace, 0.05% NaN_3). For analysis of synaptosomal Aβ concentration, RIPA extracts were assayed directly, 100 μl per well. Synaptosomal GuHCl extracts from TgCRND8 mice were diluted 1:17 with ELISA binding buffer and 120 μl of the diluted extract were added per well. For total mouse brain Aβ42, crude homogenates extracted with 6 M GuHCl were diluted 1:1000 in ELISA binding buffer and 100 μl were loaded. For quantification of total Aβ42 in exosomes, 3 μl of saline-resuspended exosome samples were combined with 15 μl of 6 M GuHCl and incubated at room temperature for 30 min. Samples were then diluted with 200 μl ELISA binding buffer and 100 μl were loaded per well.

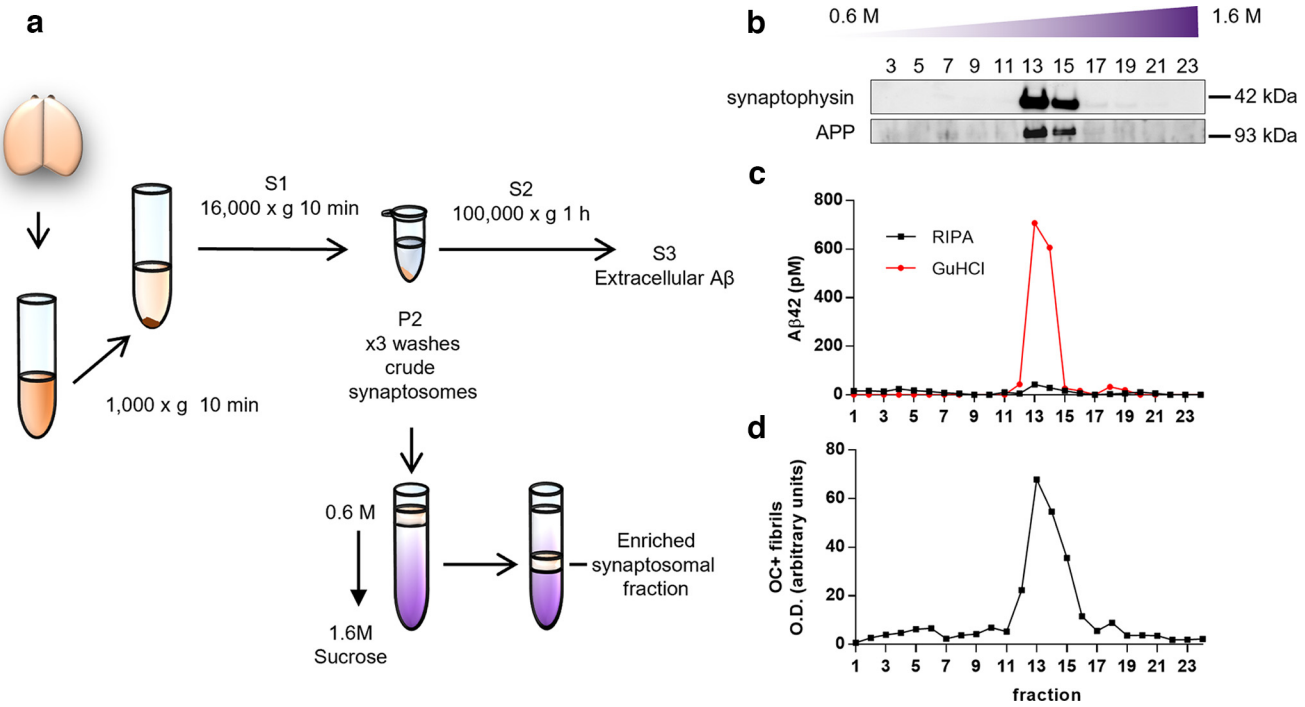

Figure 1. Accumulation of Aβ species in synaptosomes from TgCRND8 mice. ***a***, Diagram represents the preparation of synaptosomes from fresh mouse brains homogenized in 0.32 M sucrose buffer and purified in a 0.6-1.6 M continuous sucrose gradient. Fractions collected from top to bottom were pelleted and sequentially extracted with RIPA and 6 M GuHCl. ***b***, Western blotting for synaptophysin identified synaptosomes in fractions 13-15, which were also enriched in APP. ***c***, Insoluble Aβ42 (red line), measured by sandwich ELISA in GuHCl extracts, was specifically detected in synaptosomal fractions. Levels of RIPA-soluble Aβ42 monomers (black line) were low in synaptosomes, relative to the insoluble fraction. ***d***, Soluble OC-immunopositive fibrils were only enriched in the synaptophysin-positive fractions. The experiment was repeated 3 times with consistent results.

Dot blot. RIPA-extracted brain synaptosomal vesicle preparations were further diluted 1:50 in RIPA buffer, and 100 µl was applied to a nitrocellulose membrane using a dot blot apparatus. For extracellular-enriched fractions, 35 µl of sample diluted in 185 µl RIPA buffer were added per well. For exosomes, 15 µg were diluted in 200 µl of RIPA buffer and loaded. Membranes were blocked for 1 h with 5% milk and incubated overnight with the OC antiserum (1:1000; AB2286 Millipore, Sigma) that recognizes fibrillar structure over a broad size range (Kayed et al., 2007; Glabe, 2008). After washing with 0.05% Tween-20/PBS, membranes were incubated with anti-rabbit HRP conjugated secondary antibody for 1 h, washed again, and developed with ECL reagents (Millipore Sigma). Chemiluminescent signal was acquired with an ImageQuant LAS 4000 (GE Healthcare Life Sciences). Optical density was quantified with ImageJ software (National Institutes of Health) and expressed as arbitrary units.

Western blotting. RIPA buffer extracts were resolved in Novex 10%-20% Tris-tricine gels (Fisher Scientific), transferred to nitrocellulose membranes, and blocked with 5% BSA. Antibodies against AIP1/Alix (Millipore catalog #ABC40, RRID:AB_11213660), C-terminal APP (Sigma-Aldrich catalog #A8717, RRID:AB_258409), LC3B (Sigma-Aldrich catalog #L7543, RRID:AB_796155), Rab5 (Cell Signaling Technology catalog #3547, RRID:AB_2300649), Rab7 (Cell Signaling Technology catalog #12561, RRID:AB_2797956), syntaxin 1A (Cell Signaling Technology catalog #18572, RRID:AB_2798803), synaptophysin (Abcam catalog #ab8049, RRID:AB_2198854), PSD95 (Cell Signaling Technology catalog #3450, RRID:AB_2292883), and CHMP2B (Proteintech catalog #12527-1-AP, RRID:AB_10603358) were used as primary antibodies. HRP-conjugated antibodies were used as secondary antibodies and signal was developed with ECL reagents.

Electron microscopy (EM). For ultrastructural analysis, samples containing vesicles in suspension were deposited on copper grids (Electron Microscope Sciences) for 5 min followed by washing and contrasting by negative staining using uranyl acetate. Grids were imaged using a JEM 1400 transmission electron microscope (JEOL) operated at 80 kV and images were acquired with an Olympus-SIS Veleta side-mount 2K × 2K digital CCD camera.

Experimental design and statistical analysis. For longitudinal analysis of Aβ species in TgCRND8 mice (data shown in Figs. 3-6), we used a total of 106 mice (58 M/48 F) ranging in age from 3 to 17 weeks old. Because of different brain processing methodology and volume availability, sample number per Aβ measurement varied; exact numbers are stated in all figure legends. For analysis of Aβ accumulation in ECE-1-deficient mice (see Fig. 10), *Ece1* (+/+) and (+/−) littermates from 2 whole litters were used, less one mouse used instead to measure ECE-1 activity. Additional mice from a separate litter were used for ECE-1 activity measurements. For intracerebroventricular injection experiments (see Fig. 11), mice were randomized by age and sex to receive either vehicle (saline) or phosphoramidon. On graphs, each dot represents data from a single animal. Littermate WT mice ($n = 3$), or humanized *App* knock-in mice, were used to establish specificity of immunoassays and, where applicable, average results are shown on graphs as a gray line. Statistical analysis, data graphing, linear regression, and nonlinear regression were performed with Prism 7 (GraphPad Software). Total Aβ42 and synaptosomal Aβ42 levels were best fit to a sigmoidal dose–response with variable slope, and dotted lines on graphs indicate the 95% CI. For column graphs, column bars represent mean ± SEM. For comparison of three or more groups, data were analyzed by ANOVA followed by Holm–Sidak's multiple comparisons post-tests. Multiplicity-adjusted p values are indicated on graphs. For experiments with two groups, data were analyzed using unpaired Student's t test with significance set at $p < 0.05$.

Results

Production and accumulation of Aβ in synaptic endosomes

To characterize the accumulation of Aβ species within synapses, we used synaptosomal preparations from TgCRND8 mice, a model that expresses human APP with two familial AD-associated mutations (KM670/671NL + V717F) that cause Aβ42 overproduction and very early-onset amyloid deposition (Chishti et al., 2001). Synaptosomes are artificial bodies formed

by shearing neuronal processes during the homogenization of brain tissue in isosmotic buffer (Michaelis et al., 2017). They are composed of presynaptic and postsynaptic elements and have been extensively used to study synaptic physiology (Evans, 2015). Synaptosomes derived from postmortem AD brain have been shown to contain Aβ aggregates (Sokolow et al., 2012), so first we validated our experimental approach using TgCRND8 mice with abundant plaque pathology. As depicted in Figure 1*a*, material present in crude synaptosomal preparations was separated by sucrose gradient centrifugation and fractions of increasing density were collected. Synaptosome-containing fractions were identified by Western blotting for the synaptic vesicle marker synaptophysin (Fig. 1*b*). Soluble and membrane-associated Aβ species (henceforth referred to as "soluble") were extracted from each fraction with RIPA buffer, and RIPA-insoluble material was further extracted with 6 M guanidine-HCl (GuHCl) for measurement of insoluble Aβ (Fig. 1*c*). RIPA-soluble fibrillar species were quantified by dot blot with the conformation-specific OC antiserum (Kayed et al., 2007; Glabe, 2008) (Fig. 1*d*). Using this method, we found that fractions containing purified synaptosomes were selectively enriched in APP, insoluble Aβ42, and soluble fibrils. All other fractions were virtually devoid of Aβ42, indicating that the Aβ42 present in crude synaptosomal preparations from plaque-bearing mice is contained within synaptosomes and is found in an aggregated or insoluble conformation.

Next, to characterize the specific sites of synaptic Aβ accumulation, synaptosomal vesicles were released by osmotic shock (Morciano et al., 2005) and separated by density gradient centrifugation. By Western blot, we evaluated the distribution of APP and its metabolites (Fig. 2*a*) along with several synaptic and endosomal markers. Immunoreactivity for both full-length APP and APP C-terminal fragments (CTFs) closely followed the distribution pattern of early endosomal marker Rab5, consistent with APP processing in Rab5-positive vesicles. In fractions of higher density, we observed a progressive increase in the ratio of CTF-β/CTF-α, coupled with detection of CTF-γ, indications of increased amyloidogenic APP processing. With increased fraction density, there was also increased immunoreactivity for the 16 kDa LC3B protein, a marker of autophagosomes, ALG-2 interacting protein X (Alix), a cytosolic adaptor protein that regulates cargo sorting to multivesicular bodies (MVBs), and charged multivesicular body protein 2B (CHMP2B), a component of the ESCRT-II complex involved in the formation of MVBs (Henne et al., 2013). Insoluble Aβ42 levels were also more concentrated in higher-density fractions, with maximal levels in fraction 24 coinciding with the highest immunoreactivity for endosomal markers Rab5, Rab7, LC3B, Alix, and CHMP2B. These high-density Aβ accumulating fractions were not enriched in markers of synaptic vesicles (synaptophysin), synaptic plasma membranes (syntaxin), or postsynaptic densities (PSD95). For Alix, in addition to full-length protein (100 kDa), we detected a putative degradation product of ~42 kDa mostly enriched in fraction 24.

The size of vesicles contained within synaptosomes was further explored by negative-stain EM analysis of representative fractions. A synaptic marker-enriched fraction (#11) contained abundant ~100 nm vesicles, consistent with the diameter of synaptic vesicles. In contrast, within the high-density fraction (#24) strongly enriched in endosomal/autophagic markers, we found larger vesicles consistent with the size of MVBs, autophagosomes, or amphisomes (Fig. 2*b*).

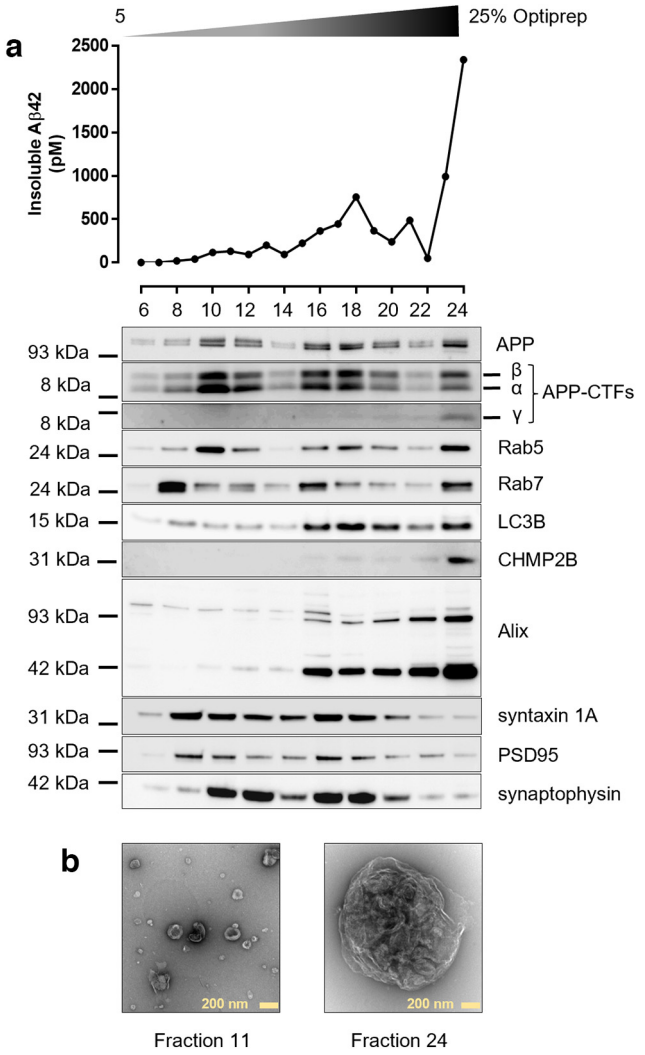

Figure 2. Preferential accumulation of intrasynaptic Aβ in Aβ-producing vesicles of endosomal origin. Synaptosomal vesicles were released from purified synaptosomes by osmotic shock and separated in a 5%-25% Optiprep gradient. ***a***, Insoluble Aβ42, measured by sandwich ELISA, preferentially localized to high-density fractions enriched in markers of endosomes (Rab5, Rab7), MVBs (CHMP2B, Alix), and autophagosomes (LC3B). Less Aβ42 accumulated in lower-density fractions enriched in markers of synaptic vesicles (synaptophysin), synaptic membrane (syntaxin 1A), or postsynaptic densities (PSD95). ***b***, Negative EM showed a representative synaptic marker-enriched fraction (#11), contained vesicles of ~100 nm, while a fraction enriched in endosomal markers (#24) contained large vesicles similar in size to MVBs, autophagosomes, and amphisomes.

Early synaptic Aβ accumulation in TgCRND8 mice

Whereas our data support that synaptic endosomes can produce and accumulate insoluble Aβ42, it has been proposed that Aβ found in synapses represents Aβ aggregates that diffuse from plaques (Koffie et al., 2009; Brody et al., 2017). Therefore, to establish how synaptic Aβ accumulates in relation to extracellular pathology, we performed a longitudinal analysis of the levels of multiple Aβ species in crude synaptosomes beginning well before the onset of amyloid plaque deposition.

First, we generated a reference dataset for the progression of amyloid pathology in TgCRND8 mice bred in our colony, by measuring total brain Aβ42 levels extracted directly from brain homogenates with GuHCl. As shown in Figure 3*a*, total brain Aβ42 levels remained stable from 3 until ~10 weeks of age, followed by a rapid accumulation phase (>10× increase) between 10 and 13 weeks, consistent with the reported onset

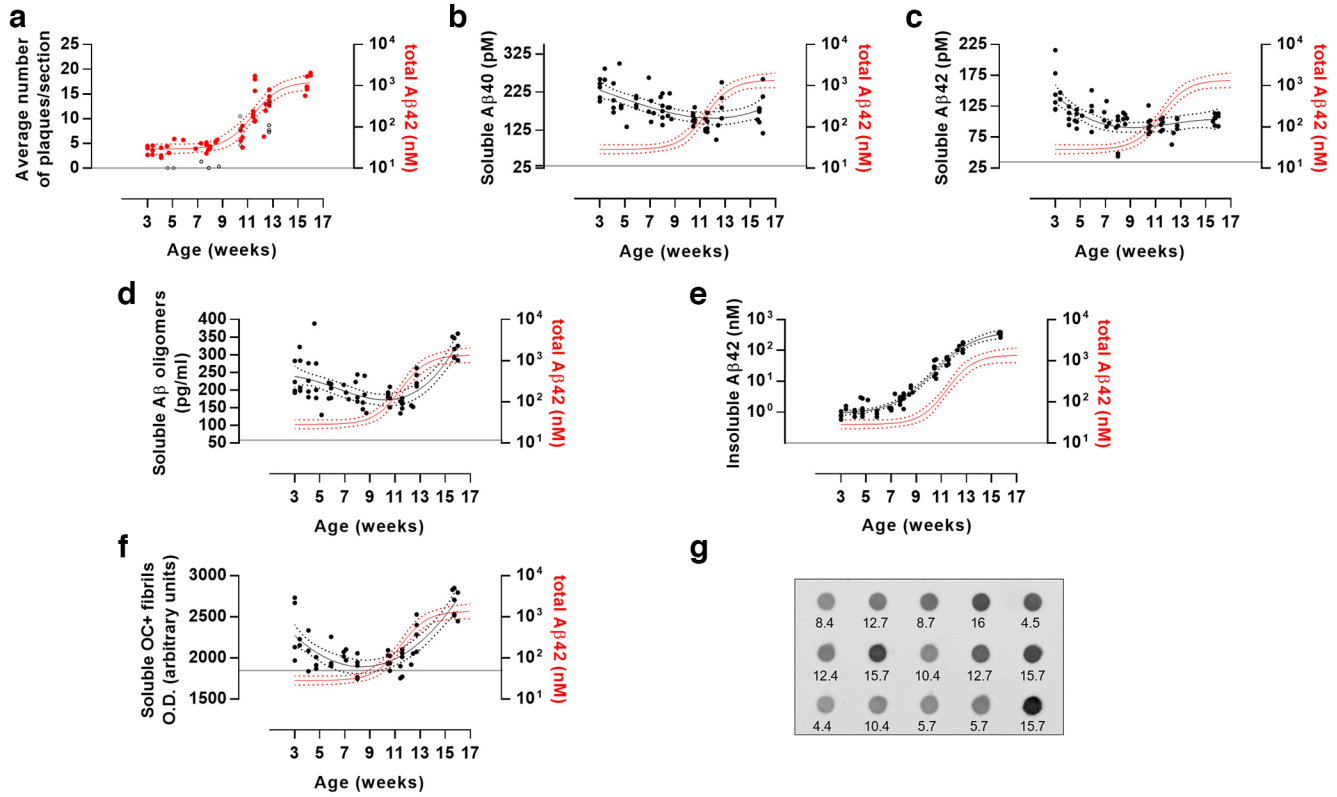

Figure 3. Alterations in intrasynaptic Aβ species before and during plaque development. ***a***, Total levels of Aβ42 in TgCRND8 mice (red circles) were best fit to a sigmoidal curve with variable slope (Hill slope of 0.3918 ± 0.1044, $R^2 = 0.8435$, red line, line also shown for reference in ***b–f***). Elevations of total Aβ42 corresponded with the increase in number of plaques per tissue section (black circles). ***b***, ***c***, Levels of synaptosomal RIPA-soluble Aβ42 and Aβ40 showed a progressive decrease from week 3 to week 11, after which levels stabilized. ***d***, Synaptosomal RIPA-soluble oligomeric Aβ showed more complex dynamics, decreasing between weeks 3 and 11, then progressively increasing from week 11 to week 16. ***e***, A time-dependent accumulation of synaptosomal insoluble Aβ42 started at 6-8 weeks of age. ***f***, Synaptosomal OC^+ fibrillar species, quantified by image analysis of dot blots, mirrored the dynamics of oligomers, with an initial decrease up to weeks 9-11 followed by an elevation from week 11 to week 16. ***g***, Representative OC dot blot image with numbers indicating age in weeks. ***b–f***, Data were fit to a third polynomial curve (solid black line). Dotted lines indicate the 95% CI. Sample sizes for specific assays were as follows: ***a***, Total Aβ42: $n = 55$, 28 M/27 F, plaques: $n = 13$, 6 M/7 F. ***b***, ***c***, RIPA-soluble Aβ42 and Aβ40: $n = 66$, 35 M/31 F. ***d***, Oligomeric Aβ: $n = 64$, 31 M/33 F. ***e***, OC^+ fibrils: $n = 54$, 28 M/26 F. ***f***, Insoluble Aβ42: $n = 73$, 39 M/34 F. Solid gray line indicates average value obtained from nontransgenic mice ($n = 3$) and represents background in human-specific Aβ40 ELISA (***b***) and background and/or endogenous rodent Aβ species in all other assays.

of extracellular amyloid plaque formation in this model (Chishti et al., 2001). Thioflavin T staining confirmed that, after 10.5 weeks of age, extracellular amyloid plaques were present in all mice (Fig. 3*a*).

Following sequential RIPA/GuHCl extraction of synaptosomes, we found that soluble Aβ40 and Aβ42 monomers, Aβ oligomers, and OC-immunoreactive fibrillar species were readily detectable in synaptosomes from 3-week-old mice (Fig. 3*b–d,f*). All of these soluble Aβ species decreased between weeks 3 and 11, while insoluble Aβ42 progressively built up (Fig. 3*e*), with a maximum increase in the rate of accumulation between weeks 8 and 12, preceding the onset of plaques by ~2 weeks. As plaque formation progressed beyond 12 weeks of age, soluble oligomers and fibrils increased (Fig. 3*d,f*), while levels of soluble Aβ40 and Aβ42 remained stable (Fig. 3*b,c*).

In interstitial fluid-enriched fractions (Fig. 4), prepared by gently homogenizing brains in isosmotic buffer without detergents and ultracentrifuged to remove EVs (S3 fraction depicted in Fig. 1*a*), we observed significant declines in all soluble Aβ species between weeks 3 and 11, closely matching those detected in synaptosomal extracts. After the appearance of plaques, extracellular Aβ levels became highly variable, potentially reflecting equilibrium between soluble and plaque-associated Aβ (Cirrito et al., 2003).

To further confirm the presence of intrasynaptic Aβ aggregates at a pre-plaque age, we additionally used a sandwich ELISA method that captures and detects with protofibril selective antibodies (Colvin et al., 2017; Grover et al., 2023). Results showed the presence of soluble Aβ protofibrils in synaptosomes from 3-week-old mice (Fig. 5). Like other soluble intrasynaptic Aβ species, the levels of Aβ protofibrils decreased over the time period leading to the buildup of insoluble Aβ42.

Accumulation of fibrillar Aβ in exosomes

Exosomes are EVs formed by the inward invagination of endosomal membranes; and, as such, they are carriers of membrane-bound Aβ produced in endosomes/MVBs (Rajendran et al., 2006; Sardar Sinha et al., 2018; Pacheco-Quinto et al., 2019) and may reflect the dynamics of intraneuronal Aβ accumulation. Using an additional set of brains, we isolated exosome-enriched EVs using a validated method that uses mild papain dissociation and sequential centrifugation to separate cellular material from EVs contained in the extracellular fluid. After further purification by density gradient ultracentrifugation (Perez-Gonzalez et al., 2017), exosome-containing fractions were characterized by Western blot, dynamic light scattering, and EM, and then the exosome-associated Aβ42 burden was determined in mice aged 4-17 weeks. In this isolation protocol, exosomes equilibrate at the 0.6/0.95 M sucrose interlayer (fractions 10-12, Fig. 6*a*), which was enriched with the exosomal marker Alix. Alix-enriched EV fractions were also enriched in APP and APP CTFs and contained particles with an average diameter of ~80.7 ± 20 nm (mean ± SD), as measured by dynamic light scattering (Fig. 6*b*). The size

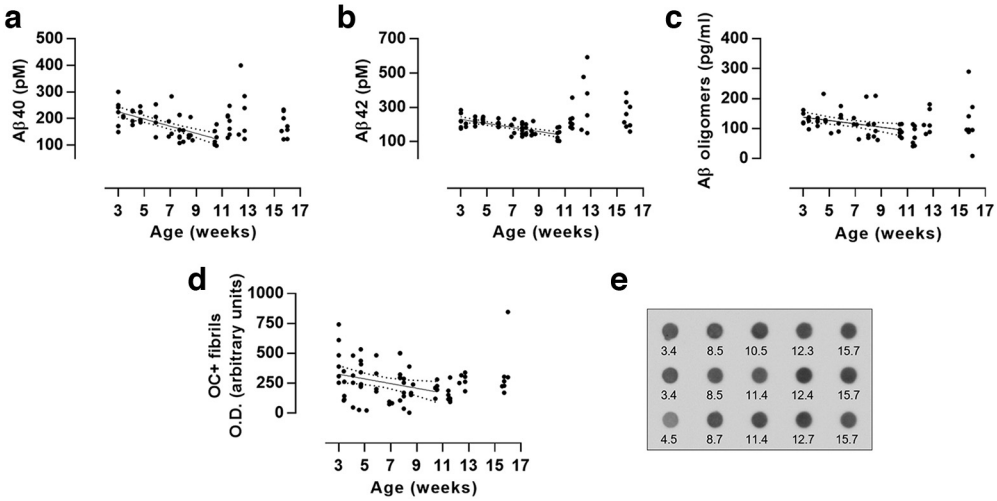

Figure 4. Age-dependent changes in extracellular Aβ species. In extracellular/interstitial fluid-enriched fractions of TgCRND8 mice before plaque deposition, there was a progressive and significant decline in levels of (***a***) Aβ40 ($r^2 = 0.435$, $p < 0.0001$), (***b***) Aβ42 ($r^2 = 0.474$, $p < 0.0001$), (***c***) Aβ oligomers ($r^2 = 0.1469$, $p = 0.0012$), and (***d***) soluble OC^+ fibrils ($r^2 = 0.0879$, $p = 0.031$). ***e***, Dot blot representative of those analyzed for OC quantification with the corresponding ages in weeks. After the onset of plaque deposition, Aβ levels followed different trends and were more variable. Data from pre-plaque mice (3-10.5 weeks old) were fit to a linear regression (solid line). Dotted lines indicate the 95% CIs. Sample sizes were as follows: ***a***, ***b***, Aβ40 and Aβ42: $n = 71$, 37 M/34 F. ***c***, Oligomeric Aβ: $n = 64$, 31 M/33 F. ***d***, OC^+ fibrils: $n = 73$, 37 M/36 F.

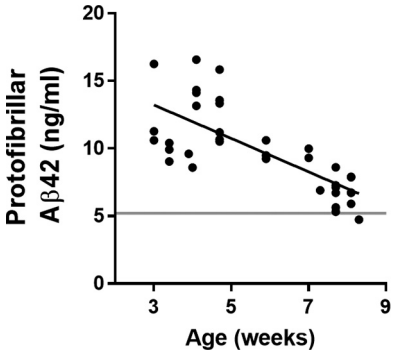

Figure 5. Detection of synaptosomal protofibrillar Aβ before the onset of plaque formation. Protofibrillar Aβ42 species, measured by sandwich ELISA in RIPA-extracted synaptosomal preparations ($n = 36$, 23 M/13F), were detectable in 3-week-old mice. Levels decreased significantly ($R^2 = 0.3462$, $p < 0.0001$) up to 8 weeks of age, when protofibrils were no longer detectable above average signal obtained with extracts from nontransgenic mice (solid gray line, $n = 3$).

range of the isolated EVs was consistent with that of exosomes, and not larger EVs, such as ectosomes (size range 100-1000 nm) or apoptotic bodies (size range 1000-5000 nm). Furthermore, the presence of the characteristic cup-shaped morphology of exosomes was confirmed by EM (Fig. 6*c*).

Aβ42 (directly extracted with GuHCl) was detectable in exosomes from very young mice and increased substantially between 11 and 17 weeks of age (Fig. 6*d*). Dot blot analysis of RIPA extracts confirmed the presence of OC-immunoreactive fibrillar species that built up over the same period (Fig. 6*e*,*f*), supporting that fibrillar Aβ accumulating in MVBs is eventually secreted in association with exosomes.

Formation and localization of intravesicular Aβ fibrils induced by protease inhibition in SH-SY5Y-APP cells

As our findings suggest that fibrillar Aβ accumulating in synaptic endosomes may have an endogenous origin, we turned to a cell culture model to further evaluate the propensity of Aβ to aggregate in Aβ-producing endosomes, and to determine whether altered proteostasis influenced this process. Using SH-SY5Y human neuroblastoma cells overexpressing WT APP (SH-SY5Y-APP), we have demonstrated that the level and state of aggregation/insolubility of Aβ produced in endosomal vesicles are dynamic and majorly controlled by the activity of phosphoramidon-sensitive proteases (Pacheco-Quinto and Eckman, 2013; Pacheco-Quinto et al., 2019). Phosphoramidon inhibits a subset of zinc metalloproteases, including Aβ-degrading enzymes ECE-1, ECE-2, neprilysin, and angiotensin-converting enzyme (Roques et al., 1993; Turner and Hooper, 2002). It does not inhibit another important Aβ-degrading metalloprotease, insulin-degrading enzyme (Farris et al., 2003). Using more selective inhibitors of neprilysin and angiotensin-converting enzyme, we have shown in previous studies that inhibition of these enzymes does not reproduce the effect of phosphoramidon treatment on Aβ levels *in vitro* or *in vivo*. More selective ECE inhibitors do, however, cause similar elevations in Aβ concentration, strongly suggesting that inhibition of ECE-1 and/or ECE-2 is at least partially responsible for the effect (Eckman et al., 2006; Pacheco-Quinto and Eckman, 2013).

Consistent with prior studies, treatment of SH-SY5Y-APP cells with phosphoramidon for 48 h led to intracellular accumulation of Aβ, measured by sandwich ELISA (Fig. 7*a*,*b*) and observed by immunocytochemistry (Fig. 7*c*) using an N-terminal Aβ antibody. The majority of Aβ42 accumulating in intracellular vesicles following phosphoramidon treatment remained in a RIPA-soluble state. To determine whether further disruption of intracellular proteolysis would drive Aβ aggregation, we treated cells with E-64, a cysteine cathepsin inhibitor that causes accumulation of APP CTF-α, -β, -γ, and other APP fragments (Pacheco-Quinto et al., 2019). By increasing accumulation of CTF-β, the immediate Aβ precursor, E-64 treatment can potentially lead to increased Aβ production in endosomal compartments also containing γ-secretase. The combination of E-64 and phosphoramidon treatment resulted in more intense Aβ immunoreactivity and the appearance of intracellular fibrils, detected by immunocytochemistry with OC antiserum (Fig. 7*c*). No immunostaining was observed in cells treated with E-64 alone, consistent with ELISA results showing no significant increase in intracellular Aβ42 concentration, and furthermore demonstrating that neither the N-terminal Aβ antibody

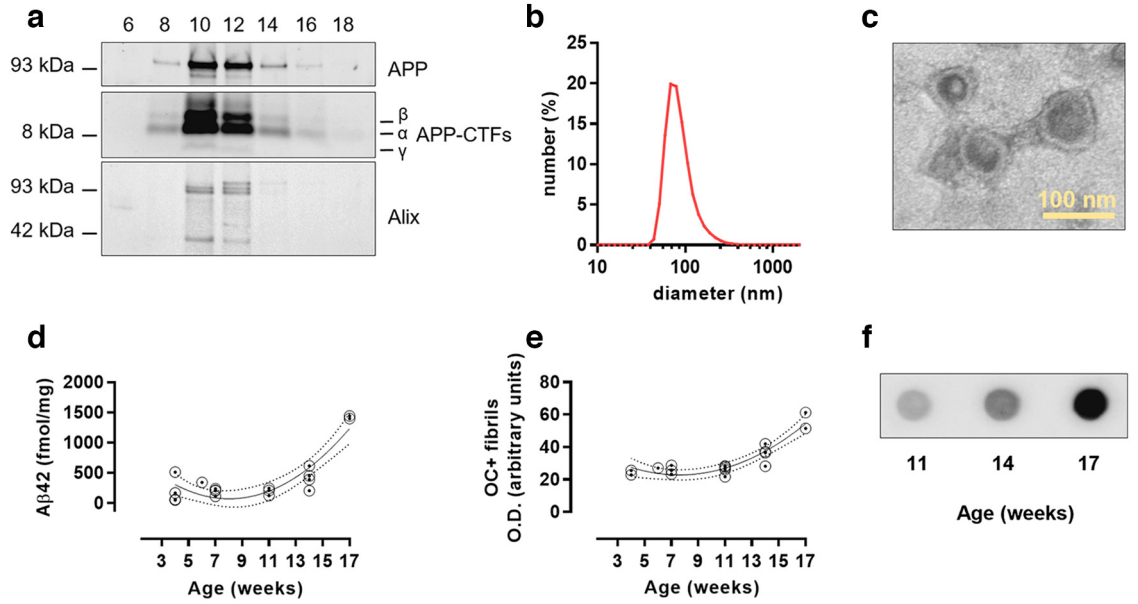

Figure 6. Age-dependent accumulation of Aβ in exosomes. ***a***, EVs, purified by density floatation, were highly enriched in the exosomal marker Alix in fractions 10-12. The exosomal fractions were also enriched in full-length APP and APP-CTFs. ***b***, By dynamic light scattering, we confirmed a homogeneous population of small EVs in pooled fractions 10-12, with a diameter of ~80.7 ± 20 nm (mean ± SD). ***c***, Negative-stain EM showed that vesicles had a cup-like shape typical of exosomes. ***d***, Total levels of Aβ42 in GuHCl-extracted exosomes progressively increased, starting at week 11 ($n = 19$, 12 M/7 F). ***e***, Levels of fibrillar species in RIPA-extracted exosomes also started accumulating after 11 weeks of age ($n = 17$, 10 M/7 F). ***f***, Representative dot blot examples for OC signal levels in 11-, 14- and 17-week-old brain-derived exosomes.

nor OC antiserum cross-reacted with APP CTFs. Results of ELISA analysis of cells extracted sequentially with RIPA followed by GuHCl showed that the combination phosphoramidon plus E-64 treatment increased soluble intracellular Aβ42 concentration ~30× compared with control cells (Fig. 7*a*). In the insoluble fraction (Fig. 7*b*), Aβ42 concentration was drastically increased >1000×, supporting that the OC^+ immunofluorescent signal represented fibrillar Aβ.

The accumulation of OC^+ fibrillar Aβ in endosomal vesicles was investigated using three different colocalization methods. First, the endocytic pathway was labeled by incubating cells with Lucifer yellow. Second, $CD63^+$ vesicles, including MVBs, were labeled by transiently transfecting cells with CD63-EGFP. Third, $Rab7^+$ vesicles, including late endosomes, were identified by immunofluorescence. In cells treated with phosphoramidon plus E-64, OC immunofluorescent signal was distributed in the endocytic pathway (Fig. 8*a*) and partially colocalized with CD63-EGFP fluorescence (Fig. 8*b*) and Rab7 immunofluorescence (Fig. 8*c*). Super-resolution Airyscan confocal images showed OC immunofluorescence arranged in a morphology highly reminiscent of intracellular vesicles, suggesting that intravesicular OC staining may localize to the rim of endosomal structures (Fig. 8*d*).

Intracellular Aβ accumulation in SH-SY5Y-APP cells with genetic deletion of *ECE1*: reproduction of the effect of phosphoramidon treatment

Without an inhibitor that selectively inhibits ECE-1 versus ECE-2, it has not been possible to determine the relative contribution of each ECE enzyme to Aβ catabolism in our cell model. To further investigate this, we knocked out *ECE1* in SH-SY5Y-APP cells and determined the effect on basal Aβ levels and response to phosphoramidon and E-64 treatment. Compared with WT SH-SY5Y-APP cells, *ECE1* KO cells had significantly elevated levels of both secreted and RIPA-soluble intracellular Aβ42 and were insensitive to phosphoramidon treatment (Fig. 9*a*,*b*). The accumulation of intracellular Aβ in *ECE1* KO cells without protease inhibitor treatment was detectable by immunocytochemistry (Fig. 9*d*); E-64 treatment resulted in a further increase in N-terminal Aβ immunoreactivity and the appearance of OC-positive signal, indicative of Aβ fibrillization. ELISA measurement of RIPA-insoluble (GuHCl-extracted) Aβ42 revealed a 20× increase in insoluble Aβ42 in E-64-treated cells compared with untreated *ECE1* KO cells (Fig. 9*c*), consistent with the immunostaining.

Synaptic Aβ accumulation in ECE-1-deficient mice

Homozygous deletion of *Ece1* in mice results in an embryonic lethal phenotype (Yanagisawa et al., 1998). Heterozygous *Ece1* KO mice, while apparently healthy, have increased endogenous Aβ levels in whole-brain homogenates (Eckman et al., 2003). To determine whether ECE-1 deficiency affects endogenous Aβ accumulation at the synaptic level, we prepared synaptosomes from heterozygous $Ece1^{tm1a(KOMP)Wtsi}$ mice that contain a "knock-out first" reporter-tagged insertion allele. Compared with littermate controls, *Ece1* (+/−) mice had a ~40% reduction in phosphoramidon-sensitive synaptosomal ECE-1 activity (Fig. 10*a*) and significantly increased endogenous synaptosomal Aβ42 concentration (Fig. 10*b*). As seen with *ECE1* KO cells *in vitro*, secreted Aβ42 and Aβ40 were also significantly elevated in extracellular (interstitial fluid)-enriched extracts from *Ece1* (+/−) mice (Fig. 10*d*,*e*).

Loss of Aβ42 proteolysis by ECE-related proteases in TgCRND8 mice

Since genetic deletion of ECE-1 triggers accumulation of endosomal/synaptosomal Aβ *in vitro* and *in vivo*, we next investigated whether the ability of ECEs to degrade intrasynaptic Aβ might be compromised in Aβ-overproducing TgCRND8 mice with aging. As previously reported and shown in Figure 11, global inhibition of ECE-related proteases by intracerebroventricular

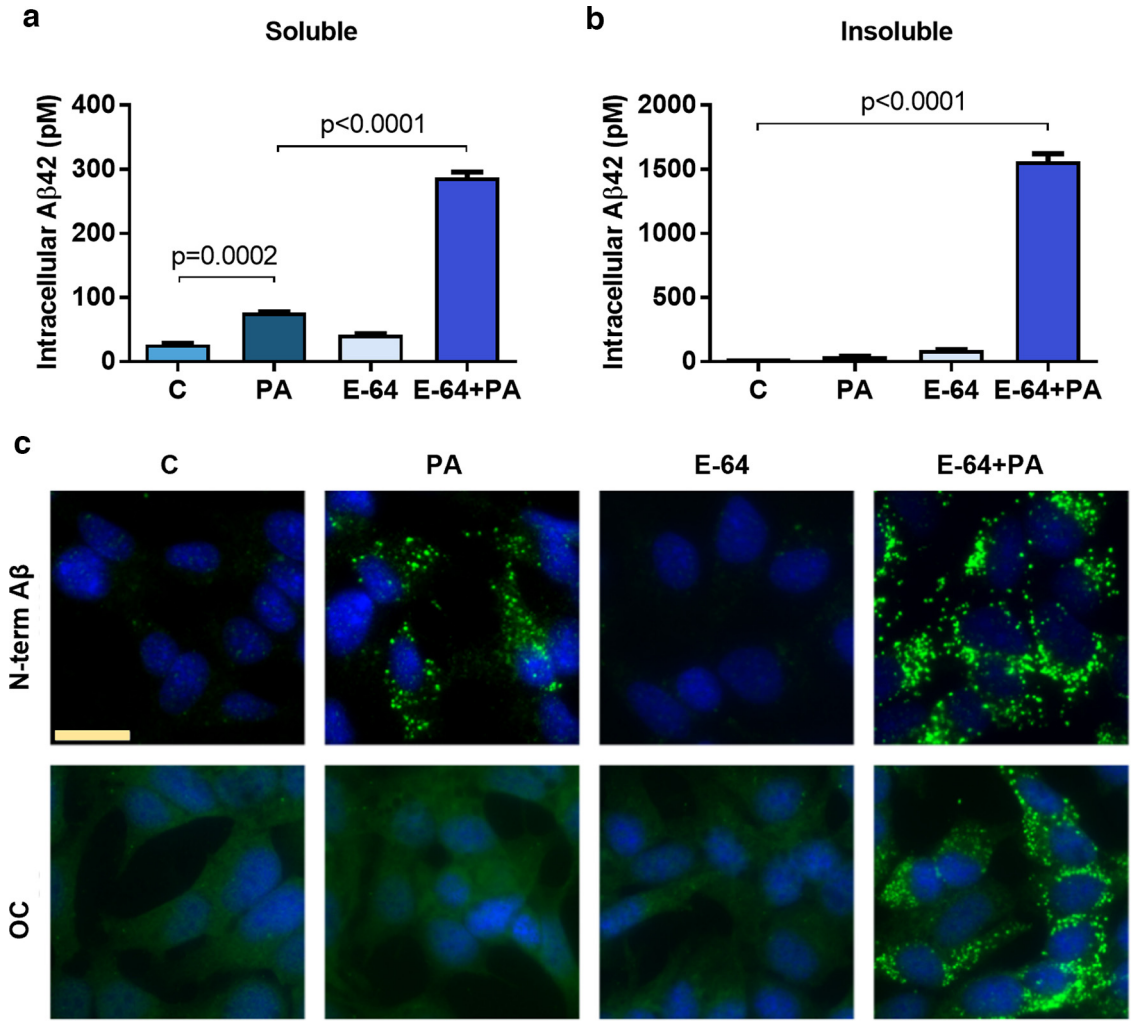

Figure 7. Intracellular accumulation of fibrillar Aβ in SH-SY5Y-APP cells. Cells were treated for 48 h with 100 μM phosphoramidon (PA) and/or 100 μM E-64 and were extracted sequentially with RIPA followed by GuHCl. ***a***, RIPA-soluble Aβ42 was significantly increased in cells treated with PA or E-64+PA, but not with E-64 alone. Combination E-64+PA treatment caused a further increase in Aβ42, compared with PA alone ($F_{(3,8)} = 705.9$, $p < 0.0001$, ANOVA). ***b***, RIPA-insoluble (GuHCl-soluble) Aβ42 was significantly increased only in cells treated with E-64+PA ($F_{(3,8)} = 666.4$, $p < 0.0001$, ANOVA). Multiplicity-adjusted p values (Holm–Sidak's) are indicated on the graphs. ***c***, Increased Aβ immunoreactivity with N-terminal Aβ antibody 33.1.1 was evident in PA and E-64+PA-treated cells, but OC-immunopositive fibrils appeared only in cells with the combined treatment. $n = 3$ for all bar graphs. Error bars indicate mean ± SEM. Scale bar, 20 μm. The experiment was repeated >3 times with consistent results.

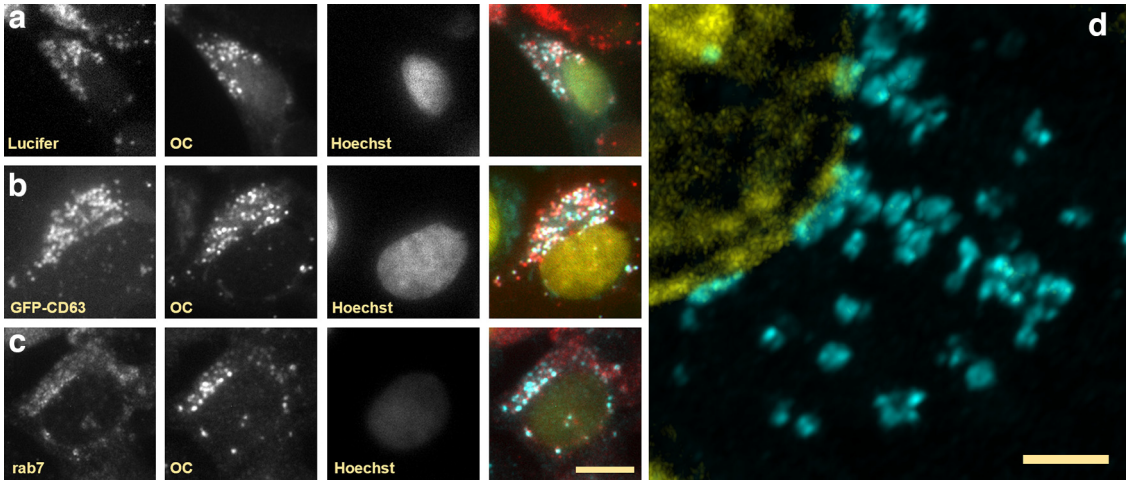

Figure 8. Association of intracellular Aβ with endosomal membranes. Immunofluorescent staining with OC anti-fibrils antiserum partially colocalized with (***a***) Lucifer yellow, labeling the endocytic pathway, (***b***) GFP-CD63, marker of multivesicular endosomes, and (***c***) Rab7, marker of late endosomes. In overlay figures, OC immunofluorescence is colored cyan blue, endosomal markers red, and nuclei yellow. ***d***, Super-resolution imaging of OC-positive fibrillar Aβ (cyan) visualized using Zeiss Airyscan confocal microscopy shows fluorescent signal presumably localized to the rim of endosomal vesicles. Scale bars: ***a–c***, 10 μm; ***d***, 2 μm.

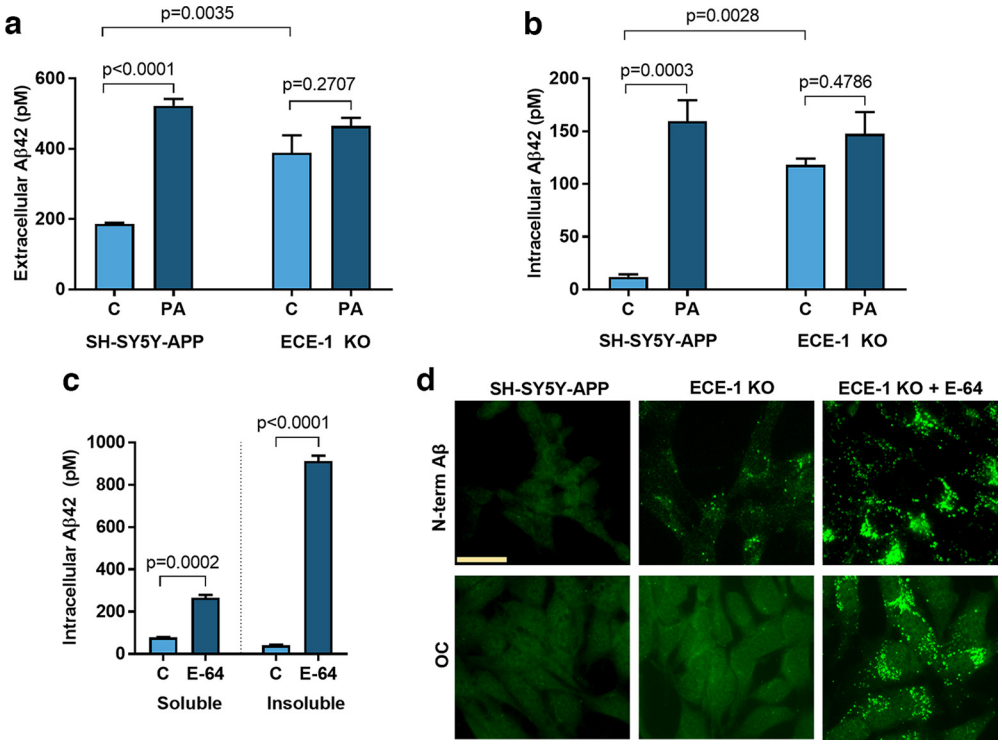

Figure 9. KO of *ECE1* in SH-SY5Y-APP cells reproduces the effect of phosphoramidon treatment. WT SH-SY5Y-APP cells and SH-SY5Y-APP *ECE1* KO cells were treated with phosphoramidon (PA, 100 μM) or E-64 (100 μM) for 48 h. Conditioned medium was collected for measurement of extracellular Aβ by sandwich ELISA. Cells were sequentially extracted with RIPA followed by GuHCl for measurement of intracellular Aβ. ***a***, ***b***, Basal levels (control [C]) of extracellular (***a***) and intracellular Aβ42 (***b***) were elevated in *ECE1* KO cells compared with WT SHSY5Y-APP cells and did not increase in response to PA, indicating that *ECE1* is the major Aβ-degrading protease in SH-SY5Y cells (extracellular: $F_{(3,8)} = 25.42$, $p = 0.0002$, ANOVA; intracellular: $F_{(3,8)} = 20.87$, $p = 0.0004$, ANOVA; multiplicity-adjusted p values indicated on the graph). ***c***, E-64 treatment alone of SH-SY5Y-APP *ECE1* KO cells produced a significant elevation of RIPA-soluble Aβ42 and elevation of RIPA-insoluble (GuHCl-extracted) Aβ42. Pairwise comparisons between untreated and treated cells made using unpaired t test. ***d***, Intracellular accumulation of Aβ in *ECE1* KO cells was confirmed by immunocytochemistry using N-terminal Aβ antibody 33.1.1. Aβ staining was substantially increased in E-64-treated cells. OC-immunopositive fibrillar species were detectable only in cells treated with E-64. Scale bar, 20 μm.

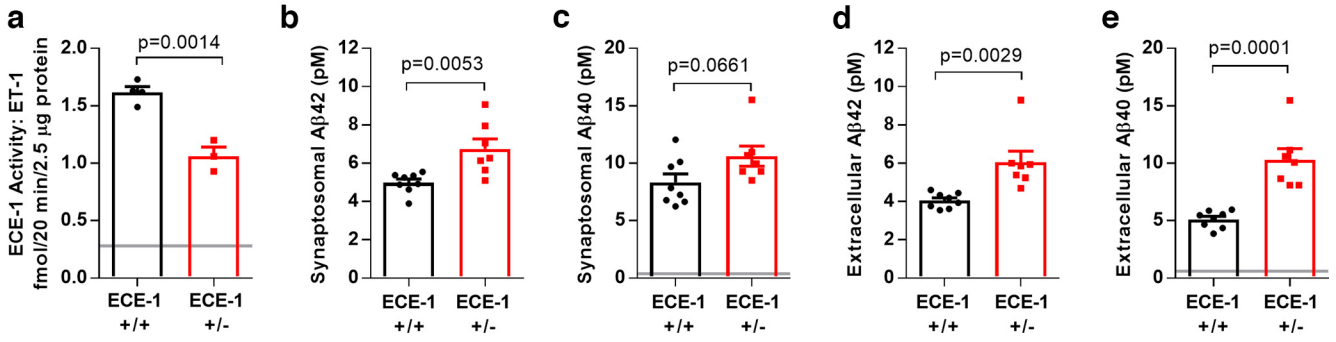

Figure 10. Endogenous synaptic and extracellular Aβ accumulation in mice with partial *Ece1* deficiency. ***a***, *Ece1* (+/−) mice ($n = 3$, 2 M/1 F) had a 40% reduction in synaptosomal *Ece1* activity compared with *Ece1* (+/+) controls ($n = 4$, 2 M/2 F), as measured with a big ET-1 conversion assay. Gray line indicates activity in the presence of ECE inhibitor phosphoramidon. ***b***, Synaptosomal Aβ42 was significantly elevated in *Ece1* (+/−) mice. ***c***, The increase in synaptosomal Aβ40 was not statistically significant. ***d***, ***e***, Both Aβ42 and Aβ40 were significantly elevated in extracellular-enriched extracts. ***c***, ***e***, Gray lines indicate average background signal from humanized *App* knock-in mice ($n = 3$) in the rodent-specific Aβ40 ELISA. Background of these samples in the rodent-specific Aβ42 ELISA was zero. Sample sizes for all Aβ measurements were *Ece1* (+/+) mice: $n = 8$, 8 M/0 F, *Ece1* (+/−) mice: $n = 7$, 5 M/2 F, aged 51 weeks. Pairwise comparisons between genotypes were made with unpaired t test.

administration of phosphoramidon causes large, rapid increases in RIPA-soluble Aβ levels, in both WT mice and in young (pre-plaque) TgCRND8 mice. Whereas the magnitude of the phosphoramidon-induced increase in synaptosomal Aβ40 was nearly identical, the increase in Aβ42 was comparatively lower in TgCRND8 mice versus WTs (Pacheco-Quinto et al., 2019). To determine whether the apparent resistance of intrasynaptic Aβ42 to degradation by ECE-related proteases was age-dependent and worsened with the development of amyloid pathology, we next compared the effect of phosphoramidon treatment on intrasynaptic Aβ42 levels at two time points: 8-10 weeks, before extracellular amyloid deposition and when insoluble synaptosomal Aβ42 was beginning to build up; and 16-17 weeks, when insoluble synaptosomal Aβ42 concentration was near maximal and stabilized, and mice had abundant amyloid plaques.

As shown in Figure 11*a*, we saw similar magnitude increases in soluble synaptosomal Aβ40 in WT and in TgCRND8 mice at pre- and post-deposition ages, indicating that phosphoramidon-sensitive

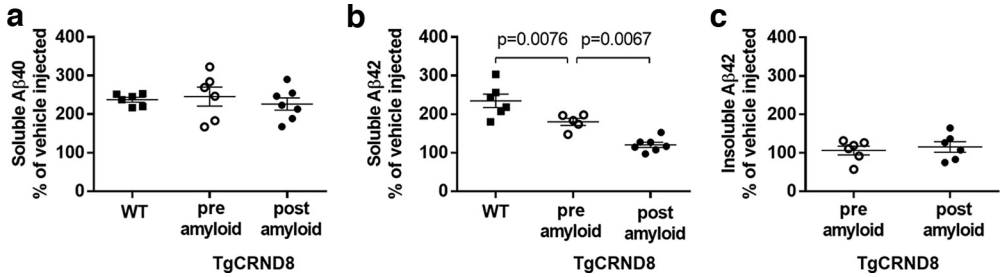

Figure 11. Sensitivity of synaptosomal Aβ40 and Aβ42 to degradation by ECE-related proteases in TgCRND8 mice, pre- and post-amyloid deposition. Mice were injected intracerebroventricularly with phosphoramidon (PA) or saline vehicle. Crude synaptosomes were isolated 16 h later and extracted sequentially with RIPA and GuHCl for measurement of Aβ by sandwich ELISA. ***a***, RIPA-soluble synaptosomal Aβ40 was elevated similarly in WT mice (WT, $n = 6$, 5 M/1 F) and in TgCRND8 mice pre-amyloid deposition ($n = 6$, 2 M/4 F, aged 8-10 weeks) or post-amyloid deposition ($n = 7$, 3 M/4 F, aged 16-17 weeks) ($F_{(2,16)} = 0.33$, $p = 0.72$, ANOVA). ***b***, There was significantly less PA-induced accumulation of RIPA-soluble synaptosomal Aβ42 in young TgCRND8 mice compared with WT mice, and a further reduction in accumulation in TgCRND8 mice after plaque deposition ($F_{(2,15)} = 24.75$, $p < 0.0001$, ANOVA). Multiplicity-adjusted p values (Holm–Sidak's) are indicated on the graph. ***c***, PA treatment did not significantly affect RIPA-insoluble (GuHCl-solubilized) Aβ42 in either age group. Data are plotted for each PA-treated group, expressed as a percent of the mean of age-matched vehicle controls which included WT ($n = 6$, 4 M/2 F), TgCRND8 pre-deposition ($n = 6$, 2 M/4 F), and TgCRND8 post-deposition ($n = 7$, 3 M/4 F). Lines indicate mean ± SEM.

Aβ-degrading activity was not compromised by mutant APP overexpression, age, or amyloid accumulation, and that Aβ40 remained in a conformation sensitive to proteolysis by ECE-related enzymes. In contrast, RIPA-soluble synaptosomal Aβ42 levels increased to a lesser extent on phosphoramidon treatment in young APP-overexpressing mice compared with WT mice (Fig. 11*b*). By 16-17 weeks, phosphoramidon produced only minimal effects on RIPA-soluble Aβ42. The RIPA-insoluble pool of synaptosomal Aβ42 was unaffected by inhibition of ECE-related protease activity at either age in TgCRND8 mice (Fig. 11*c*).

Discussion

This study provides evidence that Aβ accumulating in synapses during the progression of amyloid pathology is produced locally, within endosomal compartments. The first indication that Aβ originates endogenously at synaptic terminals is the finding that, in subfractionated synaptosomes, insoluble Aβ42 was concentrated in vesicle fractions enriched in APP, CTF-β, and CTF-γ, markers of Aβ biosynthesis. Aβ-containing fractions were also enriched in multiple markers of endosomes, autophagosomes, amphisomes, and more specifically of MVBs. Interestingly, an ~42 kDa band immunoreactive for Alix was detected both in the fraction containing the highest Aβ level (fraction 24, Fig. 2*a*) and in exosomes (Fig. 6*a*) and, by EM, we observed large (>0.5 μm) vesicles in the fraction with highest Aβ burden (Fig. 2*b*), all additional evidence suggestive of selective enrichment of MVBs in fraction 24. Morphologic characterization of ultrathin cryosections by EM may further aid in identifying the type of endosomal vesicle accumulating Aβ.

As proof that synaptic Aβ42 accumulation does not require endocytosis of plaque derived Aβ, we discovered that aggregated and insoluble Aβ was present in synaptosomes well before the emergence of extracellular amyloid pathology. In weanling mice at 3 weeks of age, synaptosomes were already enriched in soluble monomers, oligomers and fibrillar Aβ. Over the next 2 months, there was a reduction in soluble intrasynaptic Aβ species corresponding with a buildup of insoluble Aβ42, which accumulated precipitously in the weeks preceding amyloid plaque formation (~10× increased concentration between 7 and 10 weeks). The insoluble Aβ42 content of intrasynaptic vesicles then began to saturate, coinciding with increased secretion of exosome-associated fibrillar Aβ and the emergence and progression of amyloid plaques.

Although our study of intraneuronal Aβ accumulation *in vivo* was focused on synaptosomes, it is likely that similar Aβ42 accumulation may occur in endosomes in the neuronal soma. Recently, Nixon and colleagues published an immunohistochemical study demonstrating defective acidification of the E/L network in APP-overexpressing mice well before the onset of extracellular plaques (Lee et al., 2022). They further described the formation of fibrillar Aβ-filled membrane blebs of autophagic vacuoles, termed PANTHOS, surrounding neuronal nuclei, causing neuronal loss, and potentially serving as seeds for plaque formation. PANTHOS are reportedly detectable in TgCRND8 mice at ~8 weeks of age (Lee et al., 2022), corresponding closely to the onset of rapid insoluble synaptosomal Aβ42 accumulation we observed. Thus, our approach, using biochemical extraction and analysis of multiple Aβ species by ELISA and dot blot, complements immunohistochemical evidence of early intraneuronal Aβ42 aggregation preceding plaque formation in AD model mice.

With loss of Aβ42 solubility in synaptic endosomes appearing to be one of the earliest events in the development of amyloid pathology, we questioned whether disturbances in intracellular Aβ clearance pathways could be a contributing factor, focusing on the unique role of ECEs in degrading monomeric Aβ in the same compartments where the peptide is produced (Eckman et al., 2001; Pacheco-Quinto and Eckman, 2013). Comparing the effects of phosphoramidon-mediated global inhibition of ECE-related proteases on intrasynaptic Aβ content in WT mice and in TgCRND8 mice at pre- and post-plaque deposition ages, we found that the efficiency of ECEs to degrade Aβ40 (less prone to aggregation than Aβ42) was similar, indicating that enzymatic activity per se is not compromised in TgCRND8 mice. However, we discovered an age-dependent impairment in Aβ42 removal by ECE-related proteases in TgCRND8 mice. Since ECEs can degrade only monomeric Aβ in the lumen of endosomes, the most likely explanation for these results is that, in synaptic endosomes, Aβ42 specifically becomes resistant to proteolysis as amyloid pathology develops, either by quickly acquiring a nonmonomeric conformation after it is produced or by binding to membranes. This interpretation is supported by additional data showing that the insoluble pool of Aβ42 was not affected by phosphoramidon treatment. Because of the large synaptic endosomal production of Aβ42 in this mutant APP model, it is likely that nascent Aβ42 rapidly aggregates before ECEs can effectively control its accumulation. Mutations linked to familial early-onset AD that increase

Aβ42 production and accumulation in endosomes may cause pathology in humans by a similar mechanism.

Using both *in vitro* and *in vivo* KO models, our study confirms that, among the phosphoramidon-sensitive metalloproteases, ECE-1 is indeed a major player in intraneuronal Aβ homeostasis. *In vivo*, ECE-1 activity localizes to synapses and regulates endogenous intrasynaptic Aβ42 concen tration. In addition, in a cell culture model of intracellular Aβ aggregation, ECE-1 activity prevents endosomal Aβ fibrillization, even under conditions of excess Aβ production. These results, however, do not exclude a role for other ECE-related proteases in preventing intraneuronal Aβ accumulation in brain. Like *Ece1*, *Ece2* KO mice have elevated levels of endogenous Aβ in whole-brain extracts (Eckman et al., 2003). Although both enzymes are active in the endosomal pathway and hydrolyze Aβ optimally at pH ~5.5, their activities in brain are nonredundant, in part because of expression by different neuronal populations (Pacheco-Quinto et al., 2016).

Based on evidence presented in this report and in previous studies, we propose that dysfunction of ECE-1 or ECE-2 is relevant to the pathogenesis of late-onset AD. With the endosomal pathway recognized as a hub for many AD-risk associated genes, any factor altering endosomal trafficking or pH could conceivably impact ECE-mediated Aβ homeostasis and cause intraneuronal/intrasynaptic formation of Aβ aggregates. Direct genetic evidence of altered ECE function in AD is limited, but several reports show modest linkage of *ECE1* polymorphisms with AD risk (Funalot et al., 2004; Scacchi et al., 2008; Jin et al., 2009; Hamilton et al., 2012), and a recent study described a rare loss-of-function mutation in *ECE2* associated with familial late-onset AD (Liao et al., 2020). A report describing the highly polymorphic nature of CpG-CA repeats in the *ECE1*c promoter, with distinct repeat length distribution in AD patients compared with controls (Y. Li et al., 2012), is particularly intriguing in context of our data showing that partially decreased ECE-1 expression results in significantly increased endogenous synaptosomal Aβ42 accumulation.

In conclusion, our results provide evidence that pathologic Aβ species affecting synaptic function may form within synaptic endosomes early in the disease process, and perhaps independently from aggregation of extracellular Aβ. One fundamental implication of this finding is that Aβ-targeting immunotherapies may not effectively modulate this pool of intrasynaptic Aβ. Understanding the relative contributions of extracellular and intrasynaptic Aβ aggregates to cognitive dysfunction in AD is critical for the development of more effective therapies.

References

Baglietto-Vargas D, et al. (2021) Generation of a humanized Abeta expressing mouse demonstrating aspects of Alzheimer's disease-like pathology. Nat Commun 12:2421.

Billings LM, et al. (2005) Intraneuronal Abeta causes the onset of early Alzheimer's disease-related cognitive deficits in transgenic mice. Neuron 45:675–688.

Brody DL, Jiang H, Wildburger N, Esparza TJ (2017) Non-canonical soluble amyloid-beta aggregates and plaque buffering: controversies and future directions for target discovery in Alzheimer's disease. Alzheimers Res Ther 9:62.

Cataldo AM, Hamilton DJ, Nixon RA (1994) Lysosomal abnormalities in degenerating neurons link neuronal compromise to senile plaque development in Alzheimer disease. Brain Res 640:68–80.

Cataldo AM, Petanceska S, Terio NB, Peterhoff CM, Durham R, Mercken M, Mehta PD, Buxbaum J, Haroutunian V, Nixon RA (2004) Abeta localization in abnormal endosomes: association with earliest Abeta elevations in AD and Down syndrome. Neurobiol Aging 25:1263–1272.

Chishti MA, et al. (2001) Early-onset amyloid deposition and cognitive deficits in transgenic mice expressing a double mutant form of amyloid precursor protein 695. J Biol Chem 276:21562–21570.

Cirrito JR, May PC, O'Dell MA, Taylor JW, Parsadanian M, Cramer JW, Audia JE, Nissen JS, Bales KR, Paul SM, DeMattos RB, Holtzman DM (2003) In vivo assessment of brain interstitial fluid with microdialysis reveals plaque-associated changes in amyloid-beta metabolism and half-life. J Neurosci 23:8844–8853.

Colvin BA, et al. (2017) The conformational epitope for a new Abeta42 protofibril-selective antibody partially overlaps with the peptide N-terminal region. J Neurochem 143:736–749.

Eckman EA, Reed DK, Kulas JA, Ridgway EA, Amtashar FS, Combs CK, Nichols MR (2001) Degradation of the Alzheimer's amyloid beta peptide by endothelin-converting enzyme. J Biol Chem 276:24540–24548.

Eckman EA, Watson M, Marlow L, Sambamurti K, Eckman CB (2003) Alzheimer's disease beta-amyloid peptide is increased in mice deficient in endothelin-converting enzyme. J Biol Chem 278:2081–2084.

Eckman EA, Adams SK, Troendle FJ, Stodola BA, Kahn MA, Fauq AH, Xiao HD, Bernstein KE, Eckman CB (2006) Regulation of steady-state beta-amyloid levels in the brain by neprilysin and endothelin-converting enzyme but not angiotensin-converting enzyme. J Biol Chem 281:30471–30478.

Emoto N, Yanagisawa M (1995) Endothelin-converting enzyme-2 is a membrane-bound, phosphoramidon-sensitive metalloprotease with acidic pH optimum. J Biol Chem 270:15262–15268.

Evans GJ (2015) The synaptosome as a model system for studying synaptic physiology. Cold Spring Harb Protoc 2015:421–424.

Fahnoe DC, Knapp J, Johnson GD, Ahn K (2000) Inhibitor potencies and substrate preference for endothelin-converting enzyme-1 are dramatically affected by pH. J Cardiovasc Pharmacol 36:S22–S25.

Farris W, Mansourian S, Chang Y, Lindsley L, Eckman EA, Frosch MP, Eckman CB, Tanzi RE, Selkoe DJ, Guenette S (2003) Insulin-degrading enzyme regulates the levels of insulin, amyloid beta-protein, and the beta-amyloid precursor protein intracellular domain in vivo. Proc Natl Acad Sci USA 100:4162–4167.

Funalot B, Ouimet T, Claperon A, Fallet C, Delacourte A, Epelbaum J, Subkowski T, Leonard N, Codron V, David JP, Amouyel P, Schwartz JC, Helbecque N (2004) Endothelin-converting enzyme-1 is expressed in human cerebral cortex and protects against Alzheimer's disease. Mol Psychiatry 9:1122–1128.

Glabe CG (2008) Structural classification of toxic amyloid oligomers. J Biol Chem 283:29639–29643.

Glenner GG, Wong CW (1984) Alzheimer's disease: initial report of the purification and characterization of a novel cerebrovascular amyloid protein. Biochem Biophys Res Commun 120:885–890.

Gouras GK, et al. (2014) The inside-out amyloid hypothesis and synapse pathology in Alzheimer's disease. Neurodegener Dis 13:142–146.

Grover S, Pham T, Jones A, Sinobas-Pereira C, Villoch Diaz Maurino M, Garrad EC, Makoni NJ, Parks A, Domalewski RJ, Riggio G, An H, Chen K, Nichols MR (2023) A new class of monoclonal Abeta antibodies selectively targets and triggers deposition of Abeta protofibrils. J Neurochem 165:860–873.

Gyure KA, Durham R, Stewart WF, Smialek JE, Troncoso JC (2001) Intraneuronal abeta-amyloid precedes development of amyloid plaques in Down syndrome. Arch Pathol Lab Med 125:489–492.

Hamilton G, Harris SE, Davies G, Liewald DC, Tenesa A, Payton A, Horan MA, Ollier WE, Pendleton N, Starr JM, Porteous D, Deary IJ (2012) The role of ECE1 variants in cognitive ability in old age and Alzheimer's disease risk. Am J Med Genet B Neuropsychiatr Genet 159B:696–709.

Henne WM, Stenmark H, Emr SD (2013) Molecular mechanisms of the membrane sculpting ESCRT pathway. Cold Spring Harb Perspect Biol 5: a016766.

Jin Z, Luxiang C, Huadong Z, Yanjiang W, Zhiqiang X, Hongyuan C, Lihua H, Xu Y (2009) Endothelin-converting enzyme-1 promoter polymorphisms and susceptibility to sporadic late-onset Alzheimer's disease in a Chinese population. Dis Markers 27:211–215.

Kayed R, Head E, Sarsoza F, Saing T, Cotman CW, Necula M, Margol L, Wu J, Breydo L, Thompson JL, Rasool S, Gurlo T, Butler P, Glabe CG (2007) Fibril specific, conformation dependent antibodies recognize a generic epitope common to amyloid fibrils and fibrillar oligomers that is absent in prefibrillar oligomers. Mol Neurodegener 2:18.

Koffie RM, Meyer-Luehmann M, Hashimoto T, Adams KW, Mielke ML, Garcia-Alloza M, Micheva KD, Smith SJ, Kim ML, Lee VM, Hyman BT, Spires-Jones TL (2009) Oligomeric amyloid beta associates with postsynaptic densities and correlates with excitatory synapse loss near senile plaques. Proc Natl Acad Sci USA 106:4012–4017.

Langui D, Girardot N, El Hachimi KH, Allinquant B, Blanchard V, Pradier L, Duyckaerts C (2004) Subcellular topography of neuronal Abeta peptide in APPxPS1 transgenic mice. Am J Pathol 165:1465–1477.

Lee JH, Yang DS, Goulbourne CN, Im E, Stavrides P, Pensalfini A, Chan H, Bouchet-Marquis C, Bleiwas C, Berg MJ, Huo C, Peddy J, Pawlik M, Levy E, Rao M, Staufenbiel M, Nixon RA (2022) Faulty autolysosome acidification in Alzheimer's disease mouse models induces autophagic build-up of Abeta in neurons, yielding senile plaques. Nat Neurosci 25:688–701.

Li S, Selkoe DJ (2020) A mechanistic hypothesis for the impairment of synaptic plasticity by soluble Abeta oligomers from Alzheimer's brain. J Neurochem 154:583–597.

Li Y, et al. (2012) A polymorphic microsatellite repeat within the ECE-1c promoter is involved in transcriptional start site determination, human evolution, and Alzheimer's disease. J Neurosci 32:16807–16820.

Liao X, Cai F, Sun Z, Zhang Y, Wang J, Jiao B, Guo J, Li J, Liu X, Guo L, Zhou Y, Yan X, Jiang H, Xia K, Tang B, Shen L, Song W (2020) Identification of Alzheimer's disease-associated rare coding variants in the ECE2 gene. JCI Insight 5:e135119.

Michaelis ML, Jiang L, Michaelis EK (2017) Isolation of synaptosomes, synaptic plasma membranes, and synaptic junctional complexes. Methods Mol Biol 1538:107–119.

Morciano M, Burre J, Corvey C, Karas M, Zimmermann H, Volknandt W (2005) Immunoisolation of two synaptic vesicle pools from synaptosomes: a proteomics analysis. J Neurochem 95:1732–1745.

Mori C, Spooner ET, Wisniewsk KE, Wisniewski TM, Yamaguch H, Saido TC, Tolan DR, Selkoe DJ, Lemere CA (2002) Intraneuronal Abeta42 accumulation in Down syndrome brain. Amyloid 9:88–102.

Nixon RA (2007) Autophagy, amyloidogenesis and Alzheimer disease. J Cell Sci 120:4081–4091.

Nixon RA (2017) Amyloid precursor protein and endosomal-lysosomal dysfunction in Alzheimer's disease: inseparable partners in a multifactorial disease. FASEB J 31:2729–2743.

Pacheco-Quinto J, Eckman EA (2013) Endothelin-converting enzymes degrade intracellular beta-amyloid produced within the endosomal/lysosomal pathway and autophagosomes. J Biol Chem 288:5606–5615.

Pacheco-Quinto J, Eckman CB, Eckman EA (2016) Major amyloid-beta-degrading enzymes, endothelin-converting enzyme-2 and neprilysin, are expressed by distinct populations of GABAergic interneurons in hippocampus and neocortex. Neurobiol Aging 48:83–92.

Pacheco-Quinto J, Clausen D, Perez-Gonzalez R, Peng H, Meszaros A, Eckman CB, Levy E, Eckman EA (2019) Intracellular metalloprotease activity controls intraneuronal Abeta aggregation and limits secretion of Abeta via exosomes. FASEB J 33:3758–3771.

Pensalfini A, Albay R 3rd, Rasool S, Wu JW, Hatami A, Arai H, Margol L, Milton S, Poon WW, Corrada MM, Kawas CH, Glabe CG (2014) Intracellular amyloid and the neuronal origin of Alzheimer neuritic plaques. Neurobiol Dis 71:53–61.

Perez-Gonzalez R, Gauthier SA, Kumar A, Saito M, Levy E (2017) A method for isolation of extracellular vesicles and characterization of exosomes from brain extracellular space. Methods Mol Biol 1545:139–151.

Rajendran L, Honsho M, Zahn TR, Keller P, Geiger KD, Verkade P, Simons K (2006) Alzheimer's disease beta-amyloid peptides are released in association with exosomes. Proc Natl Acad Sci USA 103:11172–11177.

Ran FA, Hsu PD, Wright J, Agarwala V, Scott DA, Zhang F (2013) Genome engineering using the CRISPR-Cas9 system. Nat Protoc 8:2281–2308.

Roques BP, Noble F, Dauge V, Fournie-Zaluski MC, Beaumont A (1993) Neutral endopeptidase 24.11: structure, inhibition, and experimental and clinical pharmacology. Pharmacol Rev 45:87–146.

Roychaudhuri R, Yang M, Hoshi MM, Teplow DB (2009) Amyloid beta-protein assembly and Alzheimer disease. J Biol Chem 284:4749–4753.

Sardar Sinha M, Ansell-Schultz A, Civitelli L, Hildesjo C, Larsson M, Lannfelt L, Ingelsson M, Hallbeck M (2018) Alzheimer's disease pathology propagation by exosomes containing toxic amyloid-beta oligomers. Acta Neuropathol 136:41–56.

Scacchi R, Gambina G, Broggio E, Ruggeri M, Corbo RM (2008) C-338A polymorphism of the endothelin-converting enzyme (ECE-1) gene and the susceptibility to sporadic late-onset Alzheimer's disease and coronary artery disease. Dis Markers 24:175–179.

Scheuner D, et al. (1996) Secreted amyloid beta-protein similar to that in the senile plaques of Alzheimer's disease is increased in vivo by the presenilin 1 and 2 and APP mutations linked to familial Alzheimer's disease. Nat Med 2:864–870.

Sokolow S, Henkins KM, Bilousova T, Miller CA, Vinters HV, Poon W, Cole GM, Gylys KH (2012) AD synapses contain abundant Abeta monomer and multiple soluble oligomers, including a 56-kDa assembly. Neurobiol Aging 33:1545–1555.

Tai LM, Bilousova T, Jungbauer L, Roeske SK, Youmans KL, Yu C, Poon WW, Cornwell LB, Miller CA, Vinters HV, Van Eldik LJ, Fardo DW, Estus S, Bu G, Gylys KH, Ladu MJ (2013) Levels of soluble apolipoprotein E/amyloid-beta (Abeta) complex are reduced and oligomeric Abeta increased with APOE4 and Alzheimer disease in a transgenic mouse model and human samples. J Biol Chem 288:5914–5926.

Takahashi RH, Milner TA, Li F, Nam EE, Edgar MA, Yamaguchi H, Beal MF, Xu H, Greengard P, Gouras GK (2002) Intraneuronal Alzheimer abeta42 accumulates in multivesicular bodies and is associated with synaptic pathology. Am J Pathol 161:1869–1879.

Turner AJ, Hooper NM (2002) The angiotensin-converting enzyme gene family: genomics and pharmacology. Trends Pharmacol Sci 23:177–183.

Xu D, Emoto N, Giaid A, Slaughter C, Kaw S, deWit D, Yanagisawa M (1994) ECE-1: a membrane-bound metalloprotease that catalyzes the proteolytic activation of big endothelin-1. Cell 78:473–485.

Yanagisawa H, Yanagisawa M, Kapur RP, Richardson JA, Williams SC, Clouthier DE, de Wit D, Emoto N, Hammer RE (1998) Dual genetic pathways of endothelin-mediated intercellular signaling revealed by targeted disruption of endothelin converting enzyme-1 gene. Development 125:825–836.